See also

Seismic Structure.

Further Reading

Camfield FE (1990) Tsunami. In: Herbich JB (ed.) *Handbook of Coastal and Ocean Engineering, vol. I: Wave Phenomena and Coastal Structures*, pp. 591–634. Gulf Publishing Co.

Caminade P, Charlie D, Kanoglu U *et al.* (2000) Vanuata earthquake and tsunami cause much damage, few casualties. *EOS, Transactions of the American Geophysical Union* 81: 641.

Dudley W. and Lee M (1998) *Tsunami!*, 2nd edn. University of Hawaii.

Gonzales FI and Bernard EN (1992) The Cape Menocino tsunami. *Earthquakes and Volcanoes* 23(3): 135–138.

Gonzales FI (1999) Tsunami! *Scientific American* 21(12): 56–65.

Hokkaido Tsunami Survey Group (1993) Tsunami devastates Japanese coastal region. *EOS, Transaction of the American Geophysical Union* 74: 429.

International Tsunami Information Center (ITIC) http://www.shoa.cl/oceano/itic/frontpage.html.

Myles, D (1985) *The Great Waves*. New York: McGraw-Hill.

Voit SS (1987) Tsunamis. *Annual Review of Fluid Mechanics* 19: 217–236.

TURBIDITY CURRENTS

See **NON-ROTATING GRAVITY CURRENTS**

TURBULENCE IN THE BENTHIC BOUNDARY LAYER

R. Lueck, University of Victoria, Victoria, British Columbia, Canada

doi:10.1006/rwos.2001.0136

Introduction

Fluids do not slip at solid boundaries. The fluid velocity changes from zero to one that matches the 'far field' in a transition, or boundary, layer where friction and shear (the rate of change of velocity with distance from the boundary) are strong. The thickness of the ocean bottom (benthic) boundary layer is determined by the bottom stress and the rate of rotation of the earth. The benthic boundary layer is usually thin ($O(10\,\mathrm{m})$) compared to typical ocean depths of $\sim 4000\,\mathrm{m}$. However, in coastal regions which are shallow, and where currents and thus friction are relatively strong compared to the deep ocean, the benthic boundary layer may span most of the water column.

The boundary layer can be separated into several layers within which some forces are much stronger than others. Neglect of the weaker forces leads to scaling and parameterization of the flow within each layer. The benthic boundary layer is usually considered to consist of (1) an outer or Ekman layer in which rotation and turbulent friction (Reynolds stress) are important, (2) a very thin ($O\ (10^{-3}\,\mathrm{m})$) viscous layer right next to the boundary where molecular friction is important, and (3) a transitional layer between these, usually called the logarithmic layer, in which turbulent friction is important (**Figure 1**). The pressure gradient is an important force in all three layers. Because the velocity profile within the logarithmic layer must match smoothly with both the Ekman layer above and the viscous layer below, it will be considered last.

The Ekman Layer

Most of the open ocean is essentially frictionless, or geostrophic, and well described by a balance between the Coriolis force which pushes the flow to the right (in the Northern Hemisphere) and the pressure gradient which keeps it from veering (**Figure 2A**). This picture changes as the bottom is approached. Friction acts against the flow and decreases the velocity U. However, the pressure gradient remains and is not completely balanced by the Coriolis force fU. The current backs leftward so that friction, which is directed against the current, establishes a balance of forces in the horizontal plane (**Figure 2B**). Progressively closer to the bottom, the increasing friction slows the flow and brings it to a complete halt right at the bottom

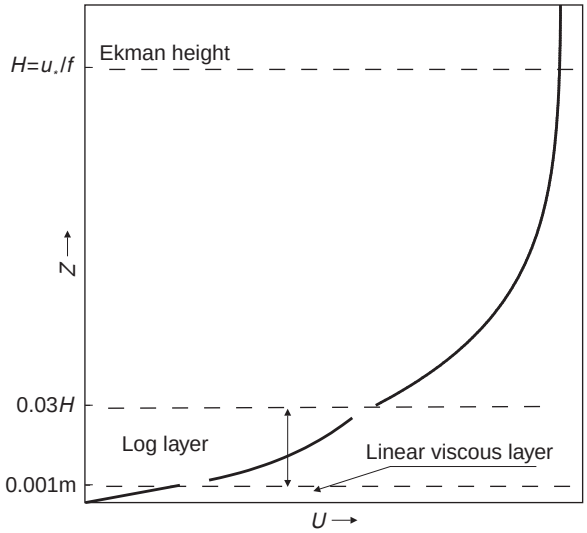

Figure 1 A conceptual sketch of the three sublayers forming the bottom boundary layer. The pressure-gradient, friction and Coriolis forces are in balance in the Ekman layer whereas only friction and pressure-gradient forces are significant in the logarithmic and viscous layers. Friction stems predominantly from the Reynolds stress of turbulence in the logarithmic layer whereas it comes mainly from molecular effects in the viscous layer.

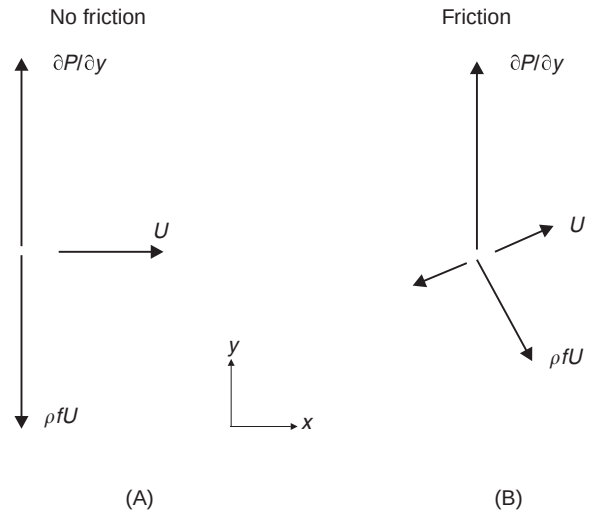

Figure 2 Plan view of the balance of forces in the geostrophic flow far above the bottom (A) and in the Ekman layer (B). The current, *U*, is directed to the right in the positive *x*-direction. Far above the bottom, the pressure gradient in the *y*-direction is balanced by Coriolis force in the opposite direction and this force is always directed to the right of the current (in the Northern Hemisphere). Within the Ekman layer, friction, τ, acts against the current. A balance of forces in both the *x*- and the *y*-directions is only possible if the current backs anti-clockwise when viewed from above.

while also further backing the flow direction. A vertical profile of the two components of the horizontal velocity might look like those depicted in **Figure 3**.

The equations of motion and their boundary conditions are

$$-fV = -\frac{1}{\rho}\frac{\partial P}{\partial x} + \frac{1}{\rho}\frac{\partial \tau_x}{\partial z}; \quad fU = -\frac{1}{\rho}\frac{\partial P}{\partial y} + \frac{1}{\rho}\frac{\partial \tau_y}{\partial z}$$
$$U = U_g, \mathrm{V} = V_g, \tau_x = \tau_y = 0 \quad \text{as } z \to \infty \qquad [1]$$
$$U = V = 0 \quad \text{at } z = 0$$

where we have assumed that the vertical velocity, *W*, is zero (flat bottom), taken the bottom at $z = 0$, assumed that both components of the stress (τ_x, τ_y) vanish far above the bottom and assigned the *x*- and *y*-components of the geostrophic velocity to U_g and V_g, respectively. The flow is geostrophic far above the bottom, that is

$$fU_g = -\frac{1}{\rho}\frac{\partial P}{\partial y}; \; -fV_g = -\frac{1}{\rho}\frac{\partial P}{\partial x} \qquad [2]$$

and if the density is homogeneous within the boundary layer, the pressure gradient is independent of height within this layer. Substituting eqn [2] into eqn [1] gives the so called Ekman equation for the boundary layer, namely

$$-f(V - V_g) = \frac{1}{\rho}\frac{\partial \tau_x}{\partial z}; \quad f(U - U_g) = \frac{1}{\rho}\frac{\partial \tau_y}{\partial z} \qquad [3]$$

It is convenient to assume that the bottom stress has no *y* component so that the bottom stress $\tau_0 = \tau_x(0)$ is directed entirely in the *x*-direction, i.e., $\tau_y(0) = 0$. Solving eqn [3] for the velocity profile requires the

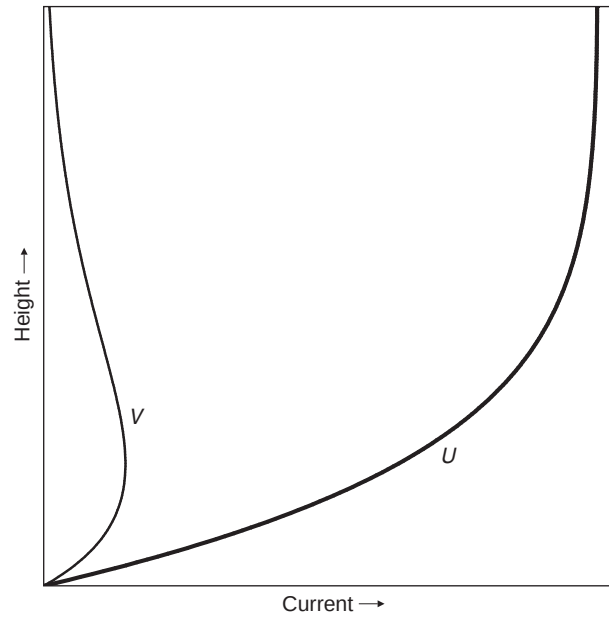

Figure 3 A conceptual velocity profile that may result from the effect of friction as depicted in **Figure 2**. A positive current component, *V*, is directed to the left of the geostrophic current.

relationship between stress and velocity, which is a major focus of boundary layer research. Fortunately, the height above the bottom over which friction is important can be determined using only dimensional analysis. For example, the x-component of velocity must be some function, F, of the parameters and variables in eqn [3] and its boundary condition $\tau_x(0) = \tau_0$, so that

$$U = F(\rho, \tau_0, f, z) \qquad [4]$$

The four variables in eqn [4] cannot all be independent. For example, ρ and τ_0 must always appear as a ratio because they are the only ones with the dimension of mass. The root of this ratio

$$u_* \equiv \sqrt{\frac{\tau_0}{\rho}} \qquad [5]$$

has dimensions of velocity and is called the 'friction velocity'. It represents a scale for the turbulent velocity fluctuations in the boundary layer. The only other independent variable is

$$H \equiv \frac{1}{f}\sqrt{\frac{\tau_0}{\rho}} = \frac{u_*}{f} \qquad [6]$$

and this is the only dimensional group that can be used to nondimensionalize z, the height above the bottom. Thus, the velocity profile must be

$$\begin{aligned} (U - U_g)/u_* &= F_u(z/H) \\ (V - V_g)/u_* &= F_v(z/H) \end{aligned} \qquad [7]$$

where the F_u and F_v are universal functions. Equation [7] is usually called the velocity defect law. The order of magnitude of the height of the boundary layer, the layer in which friction is important, is given by H and this is usually called the Ekman height. The actual height to which friction is important is within a factor of order unity of H. The Ekman height can also be considered the transition height; for $z \ll H$, friction dominates over the Coriolis force whereas above this level, the reverse holds. An important effect of rotation is that the thickness of the benthic boundary layer does not grow in the downstream direction (for uniform bottom conditions) whereas the boundary layer over a nonrotating and flat surface grows downstream.

Numerical values for the Ekman height can be derived from a traditional formulation of the bottom stress in terms of a drag coefficient, such as

$$\tau_0 = \rho C_D U_g^2 \qquad [8]$$

where the drag coefficient, C_D, must depend on the bottom characteristics, such as roughness. Typical values are $C_D \approx 0.002$. Using a geostrophic flow of $U_g \approx 0.1\,\mathrm{m\,s^{-1}}$ commonly found in the open ocean, and $f = 1 \times 10^{-4}\,\mathrm{s^{-1}}$ gives a friction velocity of $u_* = 4.5 \times 10^{-3}\,\mathrm{m\,s^{-1}}$ and an Ekman height of $H = 45\,\mathrm{m}$ which is 100 times smaller than the average ocean depth. The friction layer is thus thin compared to the ocean depth, as assumed.

Ekman solved eqn [3] almost a century ago for the special case of a stress proportional to the shear. That is,

$$\tau_x = -\rho K_V \frac{\partial U}{\partial z}; \quad \tau_y = -\rho K_V \frac{\partial V}{\partial z} \qquad [9]$$

where K_V is the eddy viscosity. The mathematically elegant spiral predicted by eqns [3] and [9] is presented in standard texts books on fluid mechanics. However, the predicted profile has never been observed and will surely remain undetected because the assumption of a constant eddy viscosity is unrealistic for turbulence close to a solid boundary (as shown below).

Viscous Sublayer

Very near a smooth bottom, $z \ll H$, a layer forms in which momentum is transferred only by molecular diffusion – a viscous sublayer. In general the stress,

$$\tau_x = \rho\nu \frac{\mathrm{d}U}{\mathrm{d}z} - \rho\overline{u'w'} \qquad [10]$$

is the sum of molecular friction which stems from the mean vertical shear (first term on the right hand side of eqn [10]) and the Reynolds stress $-\rho\overline{u'w'}$, where $\nu = \mu/\rho$ is the kinematic molecular viscosity ($\approx 1 \times 10^{-6}\,\mathrm{m^2\,s^{-1}}$). The covariance $\overline{u'w'}$ of horizontal, u', and vertical, w', velocity fluctuations leads to a transfer of momentum from the fluid towards the wall. Very near the wall vertical velocity fluctuations are strongly suppressed (no normal flow boundary condition) and the Reynolds stress is negligible compared to molecular friction.

The Ekman height, H, is not an appropriate parameter for non-dimensionalizing the height above the bottom in the thin viscous layer. Rather, the viscous scale is used:

$$\delta = \mu/u_* \qquad [11]$$

Using eqn [3] the nondimensionalized momentum balance is

$$-\frac{\delta}{Hu_*}(V-V_g)=\frac{\mathrm{d}(\tau_x/u_*^2)}{\mathrm{d}(z/\delta)}$$
$$\frac{\delta}{Hu_*}(U-U_g)=\frac{\mathrm{d}(\tau_y/u_*^2)}{\mathrm{d}(z/\delta)} \qquad [12]$$

To estimate the magnitude of the terms on the right hand side of eqn [12] the following is noted. From eqn [8], the ratio of the geostrophic speed to friction velocity is related to the drag coefficient by, $U_g/u_* = C_D^{-1/2}$ and this equals approximately 25. The velocity is at most comparable to the geostrophic velocity, so the factor $(U-U_g)/u_*$ is no more than about 25. Even for very weak flows, the terms in eqn [12] are smaller than $O(10^{-3})$. Thus, the vertical divergence of the stress is zero and the stress itself is constant.

When the stress stems entirely from molecular friction, the only possible velocity profile is a linear one that has a shear which is commensurate with the bottom stress, that is,

$$\frac{U}{u_*}=\frac{zu_*}{\nu}=z_+ \qquad [13]$$

Laboratory observations of flow over smooth surfaces show that eqn [13] holds to about $z_+ \approx 5$; this inner most region is called the viscous sublayer. A typical dimensional thickness for the viscous sublayer is $5\nu/u_* \gg 0.001\,\mathrm{m}$. Thus, this layer never extends more than a few millimeters above the bottom. Most of the ocean bottom is not 'smooth' compared to this scale.

The Wall Layer

Further above the bottom but still well below the Ekman layer, for $\nu/u_* \ll z \ll H = u_*/f$, neither the Ekman height, H, nor the molecular viscosity, ν, can be relevant parameters controlling the velocity profile. The only parameter that can non-dimensionalize the vertical height is either the thickness of the viscous sublayer or the characteristic height of bottom roughness features, z_0. Equation [12] is still the appropriate nondimensional momentum balance if z_0 is substituted for δ. The left hand side of eqn [12] is no longer as small as for the viscous sublayer but it is still small compared to 1, and the stress can be taken as constant. Thus, the wall layer and the viscous sublayer are usually called the constant stress layer. The stress eqn [10], however, is now entirely due to the Reynolds stress. Because the bottom stress has no component in the y-direction, there is also no bottom velocity in this direction.

The only parameters that control the velocity profile are the bottom stress and the roughness height. On purely dimensional grounds, we have near the wall:

$$V/u_* = 0$$
$$U/u_* = g_2(z/z_0) \qquad [14]$$

where g_2 is a, yet to be determined, universal function. Equation [14] is the law of the wall for rough bottoms. The law of the wall must be matched to the velocity-defect law eqn [7] and this is usually done by matching the shear rather than the velocity itself. The result is that

$$\frac{V_g}{u_*} = -F_v(0) = -A$$
$$\frac{U}{u_*} = \frac{1}{\kappa}\ln\left(\frac{z}{z_0}\right) \qquad [15]$$
$$\frac{U_g}{u_*} = \frac{1}{\kappa}\ln\left(\frac{H}{z_0}\right) - C$$

where $\kappa = 0.4$ is von Karman's constant and atmospheric observations indicate that $A \approx 12$ and $C \approx 4$. These equations are valid for $z/z_0 \gg 1$ and $z/H \ll 1$, simultaneously. Thus, the velocity increases logarithmically with increasing height and this profile ultimately turns into an 'Ekman'-like spiral that matches the geostrophic flow at $z = O(H)$. A thin viscous sublayer may underlay this profile if the bottom is very smooth in which case z_0 is chosen to match the profile given by eqn [13] for the same bottom stress.

It is frequently convenient to express the stress in terms of an eddy viscosity and the shear such as in eqn [9]. However, a constant stress and a logarithmic velocity profile make the eddy viscosity proportional to height, namely

$$K = u_*\kappa z \qquad [16]$$

Thus, a constant eddy diffusivity is not a good model for the wall layer and may well be inappropriate in much of the Ekman layer.

The Reynolds stress in the presence of a shear leads to the production of turbulent kinetic energy within the wall layer. It is thought that almost all of the turbulent Kinetic energy is dissipated locally and that the rate of dissipation is given by

$$\varepsilon = -\overline{u'w'}\frac{\partial U}{\partial z} = \frac{u_*^3}{\kappa z} \qquad [17]$$

Thus, profiles of the rate of dissipation of kinetic energy should provide an alternate measure of the bottom stress to that which can be derived from the velocity profile.

Observations

Values of the bottom stress are required for two major purposes: as a boundary condition for flows above the bottom and for the prediction of sediment motions. The near bottom velocity profile eqn [15] provides a convenient method for estimating the bottom stress through a fitting of U against the logarithm of z. This profile method is the one most frequently used to estimate the bottom stress. Point current meters have been placed within a few meters of the bottom and, under the assumption that they are within the logarithmic region, the bottom stress was estimated from as few as a pair of current meters. Some bottom velocity 'profile' measurements were accompanied by concurrent measurements of the turbulent fluctuations of along-flow and vertical velocity components. The covariance of these fluctuations, $-\rho\overline{u'w'}$, is an unambiguous measure of the Reynolds stress and, when this stress is extrapolated to the bottom, it usually agrees closely with the stress (ρu_*^2) inferred from the slope of the logarithmic velocity profile.

Taking profiles of velocity within the benthic boundary layer is very difficult. Consequently, there is very little observational evidence on the form of the velocity profile. One of the best deep-ocean velocity profiles was taken in the North Atlantic Western Boundary Current over the Blake Outer Ridge and reached to within 5 m of the bottom (**Figure 4**). The potential density was homogeneous within 250 m of the bottom and so the pressure gradient was independent of height as assumed in eqn [3]. The current in the upper parts of the homogeneous layer was $0.22\,\mathrm{m\,s^{-1}}$ and directed along the isobaths (approximately southward). The along-slope current had a very slight maximum at 40 m, decreased sharply below 15 m and dropped to $0.18\,\mathrm{m\,s^{-1}}$ at 5 m. The full decay to zero current at the bottom was not resolved for instrumental reasons. The cross-slope current was negligible further than 50 m above the bottom. It increased to $0.025\,\mathrm{m\,s^{-1}}$ at 5 m and was consistently directed to the left of the along-slope current (approximately eastward). The veering of the velocity vector with height above the bottom was like that depicted in **Figures 2** and **3** and reached a maximum of 8° at the lowest observation located at 5 m. Simultaneous measurements of the rate of dissipation of turbulent kinetic energy indicate that the turbulence was negligible for heights greater than 50 m above the bottom. The dissipation rate decreased monotonically with increasing height up to 50 m. Above this height, it was small and fairly uniform. Thus, the frictional layer was 50 m thick and 5 times thinner than the homogeneous layer. It is common to find different heights for the homogeneous (mixed) and the turbulent (mixing) layers. The height of the Ekman layer, H, predicted by eqn [6] was 120 m and the actual height to which friction was important was close to the expected value of $\kappa H = 50$ m, where $\kappa = 0.41$ is the von Karman constant.

The height of the logarithmic layer (eqn [15]) has not been extensively surveyed and based on the scaling arguments it must be small compared to the Ekman height. Measurements in a tidal channel indicate that profiles depart from a logarithmic form at about 3–4% of the Ekman height. The height of the constant stress layer cannot be greater than the logarithmic profile height.

For horizontally homogeneous bottom roughness, such as flat sand and fine gravel, the roughness height, z_0, is approximately 30 times smaller than the actual roughness. The notion is that the velocity profile reaches zero somewhere below the highest bottom features. Thus, there must be considerable local variations of the velocity profile for heights less than $z \approx 30z_0$ and eqn [15] represents a horizontally averaged velocity profile. The constancy of z_0 is not well established for any particular site nor does it increase consistently with increasing bottom roughness. A systematic decrease in z_0 with increasing speed above $0.2\,\mathrm{m\,s^{-1}}$ has been found and this

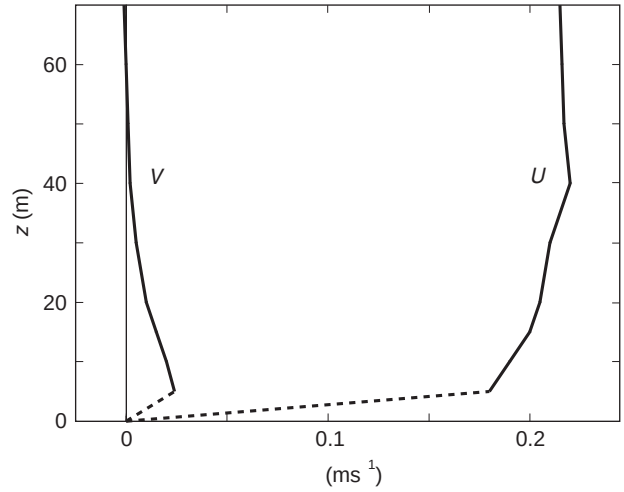

Figure 4 A sketch of the along-, U, and across-isobath, V, flow over the Blake Outer Ridge in the North Atlantic Western Boundary Current as reported by Stahr and Sanford (1999). Dashed lines within 5 m of the bottom are hypothetical extensions.

has been attributed to the onset of sediment motions and its smoothing effect on the bottom.

The bottom roughness is seldom horizontally homogeneous and the major contribution to roughness comes from bedforms (ripples and sand waves, for example) and other features with horizontal scales far greater than the largest pieces of bottom material. Thus, bottom profiles well above $z \approx 30z_0$ should show horizontal variations (**Figure 5**). For example, a wavy bottom may appear locally to have a roughness scale commensurate with the bottom material (such as sand) but, at a height comparable to the amplitude of sand waves, the bottom turns 'rough' as the turbulent eddies respond to the larger horizontal-scale structures on the bottom and not just the local features. Additional drag will be exerted on the flow by the pressure differences across sand waves (or other obstacles) due to stream-line asymmetry and outright flow separation when the slope on the lee side of objects is very steep. This is usually labeled form drag due to its similarity to the drag on bluff bodies. This feature was first observed in 1982 in profiles taken over the continental shelf off Oregon. Two logarithmic layers with differing slopes were found (**Figure 6A**). The lower layer extended to 0.1 m, and its logarithmic slope implies a friction velocity of $u_* = 0.004\,\mathrm{m\,s^{-1}}$. This layer appears to be associated with skin friction over a fairly smooth surface. The upper layer reached to at least 0.2 m and its much greater slope is indicative of stress due to form drag. More recent and much more extensive measurements in a tidal channel show a similar double logarithmic velocity profile (**Figure 6B**). The slope increased by a factor of 2 near 4 m. Span-wise oriented sand waves of 0.3 m amplitude and 16 m wavelength were present but with heights much smaller than 4 m. The effect of long horizontal-scale features on the flow over the bottom is still being investigated.

An alternate method of estimating the bottom stress is provided by the dissipation profile technique eqn [17]. Profiles of the rate of dissipation have verified the inverse height dependence predicted by eqn [17] for heights of up to 10 m. However, when the estimates of bottom stress derived from dissipation profiles are compared to the stress estimated from a fit of the velocity profile to a logarithmic form, the dissipation based estimates are typically three times smaller. Momentum budgets for bottom streams such as the Mediterranean outflow are consistent with the drag determined from the velocity profile but not with the drag inferred from dissipation profiles. There is still no satisfactory explanation for such discrepancies.

Discussion

The oceanic bottom boundary layer is a thin region of strong shear and friction with a characteristic height $H = u_*/f$, the Ekman height, that extends some 10–50 m above the bottom. A logarithmic

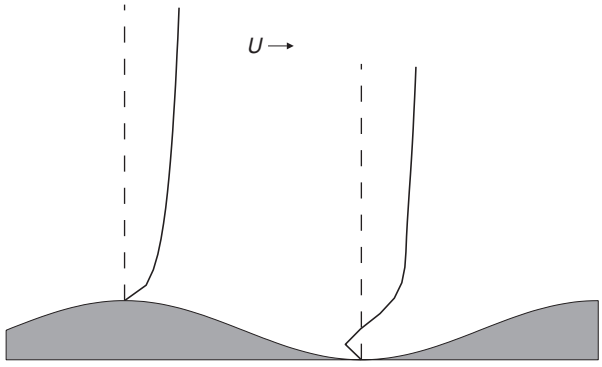

Figure 5 Conceptual sketch of spatial variations in the vertical profile of velocity over bedforms with long horizontal scales, such as sand waves. The vertical and dashed lines give a zero-velocity reference. The flow accelerates and streamlines compress on the 'up-wind' side of crests and the flow decelerates and its streamlines dilate on the lee side. This causes a pressure drop in the flow direction. If slopes are steep, flow separation and back flow may occur in the troughs and over the lee sides as depicted for the right profile.

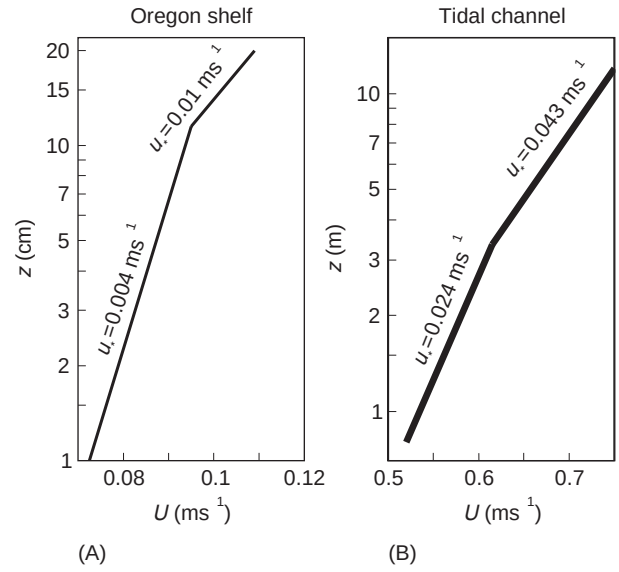

Figure 6 A sketch of velocity profiles plotted against the logarithm of height above the bottom based on data reported by Chriss and Caldwell (1982) (A) and Sanford and Lien (1999) (B). Approximately ten data points were available for each regression in (A) whereas data from about 100 different depths were used for (B). Both profiles imply a factor of 2 jump in friction velocity and a factor of 4 increase in stress for the upper logarithmic layer compared to the lower layer.

velocity profile usually exists in the lower few percent of the Ekman height and the slope of this profile can be used to infer the bottom stress. It has only recently become feasible to make detailed vertical velocity profiles and these reveal two logarithmic regions. The inner layer is controlled by the very local characteristics of the bottom and its slope gives the stress experienced by particulates on the bottom. The outer layer reveals the large addition of form drag due to long horizontal-scale bottom features and this drag provides the boundary condition for the flow well above the bottom. That is, circulation models should use a drag coefficient consistent with the friction velocity derived from the outer layer. The outer layer may be important to sedimentation after the onset of suspension.

See also

Ekman Transport and Pumping.

Further Reading

Cheng RT, Ling C-H and Gartner JW (1999) Estimates of bottom roughness length and bottom shear stress in South San Francisco Bay, California. *Journal of Geophysical Research* 104: 7715–7728.

Chriss TM and Caldwell DR (1982) Evidence for the influence of form drag on bottom boundary layer flow. *Journal of Geophysical Research* 87: 4148–4154.

Johnson GC, Lueck RG and Sanford TB (1995) Stress on the Mediterranean outflow plume: Part 2. Turbulent dissipation and shear measure-1ments. *Journal of Physical Oceanography* 24: 2072–2083.

Sanford TB and Lien R-C (1999) Turbulent properties in a homogeneous tidal bottom boundary layer. *Journal of Geophysical Research* 104: 1245–1257.

Stahr FR and Sanford TB (1999) Transport and bottom boundary layer observations of the North Atlantic deep western boundary current at the Blake outer ridge. *Deep-Sea Research* 46: 205–243.

TURBULENCE SENSORS

N. S. Oakey, Bedford Institute of Oceanography, Dartmouth, Nova Scotia, Canada

doi:10.1006/rwos.2001.0325

Introduction

This article describes sensors and techniques used to measure turbulent kinetic energy dissipation in the ocean. Dissipation may be thought of simply as the rate at which turbulent mechanical energy is converted into heat by viscous friction at small scales. This is a complicated indirect measurement requiring mathematical models to allow us to envisage and understand turbulent fields. It will require using this theory to understand how sensors might be developed using basic principles of physics to measure properties of a turbulent field to centimeter scales. Instruments must be used to carry these sensors into the ocean so that the researcher can measure its turbulent characteristics in space and time. It is also this sensor–instrument combination that converts the sensor output into a quantity, normally a voltage varying in time, that is used by the experimenter to calculate turbulent intensity. Thus, both the characteristics of sensors and the way in which the sensor–instrument combination samples the environment must be understood and will be discussed below.

Understanding Turbulence in the Ocean

There is no universally accepted definition of turbulence. Suppose that one stirs a bowl of clear water and injects some colored dye into it. One sees that filaments of dye become stretched, twisted and contorted into smaller and smaller eddies and eventually the bowl becomes a uniform color. This experiment leads to one definition of turbulence. It includes the concept that eddies in the water are distributed randomly everywhere in space and time, that energy is transferred from larger to smaller eddies, and that over time the mean separation of the dyed particles increases. In contrast, the ocean is typically stratified through a density that is determined by the temperature and salt in the water as well as the pressure. In this environment, a vertical shear in the velocity in the water column can be large enough to overcome the stability. Energy from the mean flow is converted into large-scale eddies determined by flow boundary conditions that characterize turbulent kinetic energy at its maximum scales. Further vortex stretching creates smaller and smaller eddies resulting in a turbulent cascade of energy (velocity fluctuations) to smaller scales until viscous forces begin to dominate where the energy is eventually dissipated as heat. This article focuses on sensors to measure this dissipation process directly by measuring the effect of viscosity on the turbulent cascade.